Supplemental Information

CONVENTIONS

We consider 'generic' vertices where the sector angles meet three conditions: (i) no two angles are equal, (ii) no pairs of adjacent angles add to π, and (iii) all angles are less than π. We maintain a counter-clockwise orientation of the vertex and define the fold angles with respect to the right hand rule; positive/negative folding angles correspond to 'valleys/mountains'. We routinely denote MV patterns by the four signs of ρ_i (*e.g.* $\{+,-,-,-\}$), keeping in mind that all vertices exhibit fold-inversion symmetry—if $\{\rho_i\}$ is a valid fold configuration, so is $\{-\rho_i\}$. The two branches of folding motion of generic Euclidean 4-vertices each correspond to a MV pattern with three folds of the same sign and one 'unique' fold with the opposing sign (Fig. 1a). Which two folds can be unique follows from inequalities [5, 18] of the sector angles α_i. We orient Euclidean vertices such that folds 1 and 2 are the unique folds and such that $\alpha_2 > \alpha_4$. When working with non-Euclidean vertices derived from shrunken or expanded Euclidean ones, we maintain this designation for the folds. These conventions ensure that the generic features of branches and folding curves are preserved for generic vertices. Specifically, the slopes $d\rho_j/d\rho_i$ are maintained, as well as the structure of the branches I and II (and subsequently A, B, C, and D for non-Euclidean vertices).

GEOMETRY OF NON-EUCLIDEAN 4-VERTICES

Mountain-Valley arrangements.— We now determine which MV patterns can arise in non-Euclidean 4-vertices, both for $\varepsilon < 0$ and $\varepsilon > 0$. To systematically map out all possibilities, we represent generic 4-vertices (Euclidean or non-Euclidean) as spherical linkages, mapping each fold i to a point x_i on the Euclidean sphere S and connecting these points by geodesic arcs of length α_i [41]. We then randomly place the four points x_i on the sphere [Fig. 1(a)]. For clarity, we represent the sphere S on flat paper with the Mercator mapping [Fig. 1(b)]. Without loss of generality we start with x_1, x_2 and x_3 and their antinodal points x_i'. For definiteness, we first assume that $\rho_2 > 0$—the case $\rho_2 < 0$ is related by fold inversion symmetry. We focus on sector angles $\alpha_i \leq \pi$, connect x_1 and x_2 by their shortest geodesic arc, $\overline{x_1x_2}$, and indicate the great circle coincident with this arc, C_{12}. We then repeat this procedure for the pairs x_1/x_3 and x_2/x_3. The great circles C_{12}, C_{13} and C_{23} partition S in 8 triangular sectors labeled $(c-j)$ (Fig. 1b). Irrespective of our choice of x_1, x_2 and x_3, a definite MV pattern emerges when x_4 is placed in any of these sectors, as the great circles determine the sign of ρ_i. In particular, we find that $\rho_1 > 0$ when $x_4 \in \{d,e,g,j\}$ and $\rho_1 < 0$ otherwise; $\rho_3 > 0$ when $x_4 \in \{c,d,g,i\}$; $\rho_4 > 0$ when $x_4 \in \{c,e,g,h\}$. Taken together, and reintroducing fold-inversion symmetry by relaxing the condition $\rho_2 > 0$, we find the full list of possible mountain valley assignments, accounting for relabeling symmetries (*i.e.*, $\rho_i \leftrightarrow \rho_{i+1}$ etc) (see Suppl. Table 1). In sectors (c,d,e,f), we find 'bird foot' configurations ($\{\pm,\mp,\mp,\mp\}$); in sector (g) we find 'bowls' and 'cones' ($\{\pm,\pm,\pm,\pm\}$), and in sector (h) we find 'saddles' ($\{\pm,\mp,\pm,\mp\}$). Finally, the vertices obtained by placing x_4 in sectors (i,j) correspond to ($\{\pm,\pm,\mp,\mp\}$) but necessarily involve self-intersections, that can only be circumvented when we allow $\alpha_i > \pi$.

The location of x_4 restricts the value of ε in some sectors (see Suppl. Table 1).. First, we note that the angular surplus has no fixed sign in cases (c-f), which implies that non-Euclidean vertices can have the standard 'Huffman' motif, as expected from continuity. However, one can show that in sector (g), $\varepsilon < 0$, whereas in sector (h), $\varepsilon > 0$. To determine the sign of the angular surplus for vertices in configuration (g) and (h), we proceed as follows. First, given a spherical triangle ABC and a point D within this triangle, we note that $AD + DC < AB + BC$. For case (g), the relevant triangle is span by x_1, x_3 and x_2', and so it follows that $x_1x_4 + x_4x_3 < x_1x_2' + x_2'x_3$. Hence, it follows that the sum of the sector angles, $x_1x_2 + x_2x_3 + x_3x_4 + x_4x_1 < x_1x_2 + x_2x_3 + x_1x_2' + x_2'x_3$; by definition, $x_1x_2 + x_1x_2' = \pi$ (and permutations thereof), so that we find for case (g) that $x_1x_2 + x_2x_3 + x_3x_4 + x_4x_1 < 2\pi$, and hence $\varepsilon < 0$.

For case (h), we note that $x_1x_4 > x_1x_2'$ (otherwise point 4 would have been in triangle (c), (i), (d) or (g)), and similarly, $x_3x_4 > x_3x_2'$. Hence $x_1x_2 + x_2x_3 + x_3x_4 + x_4x_1 > x_1x_2 + x_2x_3 + x_3x_2' + x_1x_2' = 2\pi$, so that in case (h), $\varepsilon > 0$. For the self-intersecting cases (i) and (j), the angular surplus ε has no fixed sign.

Finally, we note that case (d) also may appear to have $\varepsilon < 0$, but this is not necessarily the case when x_1x_2 and x_2x_3 become large; indeed applying the same reasoning as above, we find that $x_1x_2 + x_2x_3 + x_3x_4 + x_4x_1 < 2\,[x_1x_2 + x_2x_3]$ which does not restrict the sign of ε.

Sector	Sign ε	$\{\rho_1, \rho_2, \rho_3\rho_4\}$	type
c	$\pm$	$\{-,+,+,+\},\{+,-,-,-\}$	birdfeet
d	$\pm$	$\{+,+,+,-\},\{-,-,-,+\}$	birdfeet
e	$\pm$	$\{+,+,-,+\},\{-,-,+,-\}$	birdfeet
f	$\pm$	$\{-,+,-,-\},\{+,-,+,+\}$	birdfeet
g	$-$	$\{+,+,+,+\},\{-,-,-,-\}$	cone
h	$+$	$\{-,+,-,+\},\{+,-,+,-\}$	saddle
i	$\pm$	$\{-,+,+,-\},\{+,-,-,+\}$	self-intersecting
j	$\pm$	$\{+,+,-,-\},\{-,-,+,+\}$	self-intersecting

SUPPL. TABLE 1. Sector location x_4, sign of ε, MV-patterns and type of 4-vertex.

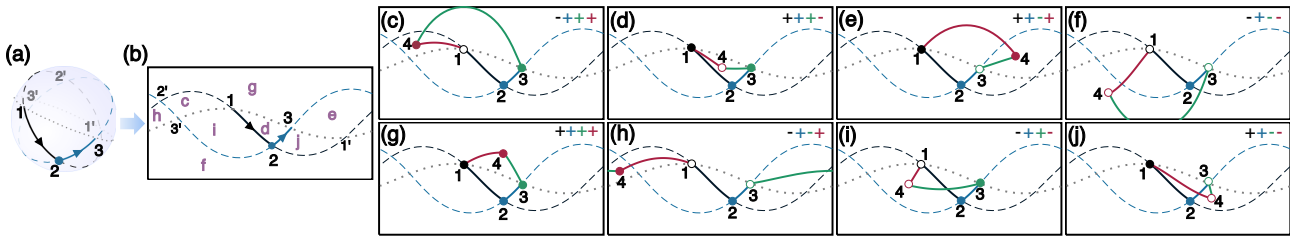

SUPPL. FIG. 1. (a) Random placement of the points x_1, x_2 and x_3, representing the folds 1, 2, and 3, on the Euclidean sphere. Also indicated are the plate edges (solid lines), antinodal points x_1', x_2', and x_3', and great arcs passing through these points (dashed and dotted lines). (b) Same as (a) but on a Mercator mapping, showing how the three great circles partition the sphere in eight spherical triangles that we label c- j. (c-j) A definite MV-pattern emerges when x_4 is placed in any one of the eight triangles (fold angle sign represented by closed/open dots).

TRISTABLE VERTEX EXPERIMENTS

Fabrication

Tristable vertices were 3D printed with a Stratasys Fortus 250 MC, which is capable of printing ABS plastic, as well as a sacrificial ABS-like plastic, with a layer thickness of 0.18 mm and an XY-resolution of better than 0.24 mm. The sacrificial material serves as a scaffold and allows us to print non-flat vertices. The scaffold is dissolved after printing by putting the structure in a 70° C NaOH solution. With this technique, we are able to print non-flat vertices with a large range of angular surplus ε.

Our vertices are 150 mm in diameter, consisting of four plates which are 3.0 mm thick. Each adjacent pair of plates is connected by hinges directly printed in a joined configuration. The hinges consist of two conical holes attached to one plate, and two opposing conical pins attached to the opposing plate. With just enough clearance to allow for rotation once extracted from the support material, no post-assembly is required. The axes of rotation of all these hinges meet at the center of the vertex. The main experimental limitation is the finite maximal folding angle (∼2.65 rad) due to the formation of self-contacts between plates for high folding angles.

Each adjacent plate pair is designed to accommodate a torsional spring in 1.14 mm diameter holes on their sides near the hinge, which can be inserted after printing. The holes for the spring are offset such that the central axis of torsional spring coincides with the axis of the hinge. As discussed in the main text and in relation to Fig. 4, we put a single torsional spring in a unique fold to make a negative surplus vertex tristable, or we put a single torsional spring in a non-unique fold to make a positive surplus vertex tristable. We note that for future applications, besides the ever-expanding range of 3D printing techniques, easily scalable techniques such as vacuum forming and thermo-molding, potentially combined with differential swelling or (heat)shrinking, could be explored to perturb initially Euclidean origami sheets towards the non-Euclidean origami envisioned here.

Measurements of Elastic Energy

To measure the energy curves for these vertices as shown in Fig. 4, we use an Instron MT-1 torsion tester with a 2.25 N·m load cell. This machine allows us to measure angular displacements with a resolution of 5×10^{-5} rad and torques with a resolution of 0.01 N·m. We have designed special grips to hold the vertex firmly on two adjacent plates while the torsion tester opens/closes the fold between them.

Converting the raw (torque) measurements from the Instron to energy curves such as those in Fig. 4 of main text is a multi-step process. First, we must determine the rest angle and spring constant of the torsional spring. We do this by gripping the vertex around the fold with the spring and performing torque vs. displacement tests opening/closing this fold. Next, we ensure that the vertex is on the bistable branch and attach it to the instron in a different orientation—this time around the fold opposite the spring. By performing torque vs. displacement tests opening/closing this fold, we probe the bistable branch. Finally, we 'pop' the vertex through to the other (monostable) branch and perform opening/closing tests on this fold to probe the monostable branch.

For all of these measurements, we must account for gravity and friction. Gravity applies a changing torque throughout the experiments on account of the evolving distribution of mass around the folding axis as the vertex opens/closes. Frictional forces arise because our hinges are imperfect, but are easy to identify/handle as they are constant, rate independent, and switch signs during opening and closing. To account for friction, we do cyclic experiments where we first increase the fold angle ρ_i to its maximum value, then decrease it to its minimum value. Since the frictional forces are always oriented opposite to the direction of motion, we average these forward/backward measurements to obtain curves with friction removed. To remove gravity, we do two separate experiments: one with the torsional spring attached to the vertex, and one with the spring removed. By subtracting these two signals, we suppress the contribution

from gravity.

After obtaining the friction- and gravity-corrected torque measurements, we simply integrate these to obtain energy curves for the different ρ_i as presented in the main text. We remark that the precise 'zero' position of the Instron has an effect on the asymmetry of the energy curves—if the Instron zero point does not coincide to with the 'true' zero point of the fold being probed, the left/right energy curves are offset during integration. We speculate this is the cause for the asymmetry in our energy curves in Fig. 4d, but leave them as is rather than (arbitrarily) picking a new gauge to make them symmetric.